

Received October 5, 2019, accepted October 31, 2019, date of publication November 5, 2019, date of current version November 18, 2019.

Digital Object Identifier 10.1109/ACCESS.2019.2951579

Convolutional Neural Network-Assisted Optical Orbital Angular Momentum Recognition and Communication

PEIPEI WANG¹, JUNMIN LIU², LIJUAN SHENG³, YANLIANG HE¹, WENJIE XIONG¹, ZEBIN HUANG¹, XINXING ZHOU³, YING LI¹, SHUQING CHEN¹, XIAOMIN ZHANG⁴, AND DIANYUAN FAN¹

¹International Collaborative Laboratory of 2D Materials for Optoelectronics Science and Technology, Engineering Technology Research Center for 2D Material Information Function Devices and Systems of Guangdong Province, Institute of Microscale Optoelectronics, Shenzhen University, Shenzhen 518060, China

²College of New Materials and New Energies, Shenzhen Technology University, Shenzhen 518118, China

³Synergetic Innovation Center for Quantum Effects and Applications, School of Physics and Electronics, Hunan Normal University, Changsha 410081, China

⁴Laser Fusion Research Center, China Academy of Engineering Physics, Mianyang 621900, China

Corresponding author: Shuqing Chen (shuqingchen@szu.edu.cn)


This work was supported in part by the National Natural Science Foundation of China under Grant 61805149, Grant 61575127, Grant 61490713, and Grant 61571188, in part by the Guangdong Natural Science Foundation Grant 2016A030310065, in part by the Program of Fundamental Research of Shenzhen Science and Technology Plan under Grant JCYJ20180507182035270, in part by the Science and Technology Project of Shenzhen under Grant ZDSYS201707271014468, in part by the Educational Commission of Guangdong Province under Grant 2016KCXTD006, in part by the International Collaborative Laboratory of 2D Materials for Optoelectronics Science and Technology under Grant 2DMOST2018003, and in part by the Hunan Provincial Innovation Foundation for post-graduate under Grant CX2018B291.

ABSTRACT The identification of orbital angular momentum (OAM) modes with high-accuracy and -speed is always a difficult issue in practically applying optical vortex beams (OVs). In this work, we propose and experimentally investigate a convolutional neural network (CNN) method for optical OAM mode identification and shift-keying (SK) communications. The CNN model, including convolution and pooling layers, was designed to extract mode information from the diffraction patterns produced by diffracting the OVs with a cylindrical lens. After trained with loads of studying samples, the CNN model has a good generation ability in recognizing the OAM modes of OVs ranging from -15 to 15 . The recognition accuracy reaches 99% with the turbulence intensity of $C_n^2 = 1 \times 10^{-13} \text{ m}^{-2/3}$, $\Delta z = 50 \text{ m}$. Even under the turbulence of $C_n^2 = 1 \times 10^{-12} \text{ m}^{-2/3}$, $\Delta z = 50 \text{ m}$, the accuracy still exceeds 89%. By mapping and encoding a Lena gray image with the size of 100×100 pixels to two OAM channels, the OAM-SK signals with 900 modulation orders were successfully demodulated by the CNN model, and the image was well recovered after transmission. With an I5-8500 Central Processing Unit, this recognition process only takes 1×10^{-3} s per mode. It is anticipated that the CNN methods might provide an effective way for identifying OAM modes with high-accuracy and -speed, which may have great potentials in OAM communication, quantum information processing, and astronomical application, etc.

INDEX TERMS Neural networks, optical vortices, optical signal detection.

I. INTRODUCTION

Optical vortex beam (OV) has attracted extensive interests due to their potential advantages in various applications [1]–[5]. The OV possessing helical phase front can be characterized by an azimuthal phase structure $\exp(i l \varphi)$ and carries orbital angular momentum (OAM) of $l \hbar$ per photon [6],

The associate editor coordinating the review of this manuscript and approving it for publication was Choon Ki Ahn .

where l is the topological charge (TC) representing the OAM mode, and φ denotes the azimuth angle in the cylindrical coordinate system. Because of the phase singularity in beam cross-section, OV shows a “dark hollow” intensity distribution. Those spatially variant field distributions reward OVs many unique optical properties, which have great potentials in the fields of particle capture and manipulation [7]–[9], optical communication [10], [11], and quantum information [12], etc. Especially for optical communications, the OVs

with different OAM modes are mutually orthogonal when l takes integers, which means that the light beam carrying OAM can provide an additional physical degree of freedom in increasing communication capacity and modulation ability [13]. By multiplexing OAM modes, the communication capacity of 2.56 Tbit/s and the spectral efficiency of 95.7 bit/s/Hz have been realized [14]. And an ultra-high-speed optical communication link with the transmission rate of 1.6 Tbit/s was also achieved by multiplexing OAM and wavelength simultaneously [15]. However, the OAM shift-keying (OAM-SK) communication manifesting as the rapid switching of OAM modes is seriously hampered for lacking effective identification methods. Moreover, atmospheric turbulence (AT) in free space will severely destroy the helical phase front of OV_s, making it difficult to recognize OAM modes and reducing the detection speed and accuracy.

The interference and diffraction methods are commonly used to detect OAM modes by converting light intensity distributions into patterns that carry significant mode features. Interfering OV_s with a plane wave, one can directly read mode information from the fork-shaped fringes of interference patterns [16], [17]. However, the fringes formed by interference are difficult to be recognized for the OV_s with large TCs because the number of fringes is proportional to the absolute value of TCs. For the grating diffraction methods, OV_s are converted to Gaussian beams and diffracted to different diffraction orders by designing forked gratings with spiral phases [18], [19]. This method also has a limit identification range because one grating structure can only detect fixed OAM modes. Aperture diffraction [20], [21] and cylindrical lens (C-lens) detection methods have high accuracy [22], [23], of which the C-lens method has a simple experimental operation and obvious OAM mode features by diffracting the OV_s to $l + 1$ stripe distributions in the focal plane. All of those methods provide effective ways to identify OAM modes. However, the identification processes are all performed based on image recognition and classification, which depends heavily on the resolution limit of observer and makes the practical identification seriously restricted in speed and accuracy. Furthermore, when the OV propagate in free space, its spiral phase structure is easily distorted by AT, resulting in mode dispersion and intensity distribution distortion. This distortion will further disturb the interference and diffraction patterns and limit the OAM mode recognition range, accuracy, and speed.

The key to detecting OAM modes is the identification and classification of intensity patterns, which is where the convolutional neural network (CNN) excels. Owing to the powerful data processing capability, CNN has been widely used in computer vision [24], language processing [25], [26], and optical information processing [27]–[30], etc. Researchers have also used deep neural networks to identify conjugated OAM modes and achieved an accuracy of 74% [31], which can be further increased to exceed 90% by using CNN [32]. These studies indicate that the CNN based OAM mode iden-

tification methods have a high recognition accuracy. However, the scheme can only identify limited modes, and it is difficult to identify the modes that are mutually conjugated with no significant difference in light intensity distributions. In optical OAM communications, eliminating non-conjugate modes seems a big waste of multiplexing resources. Therefore, a method that can well recognize a wide range of OAM modes with high accuracy and speed and has a certain anti-turbulence capability is still urgently required.

In this article, we propose and experimentally demonstrate a CNN method for OAM mode recognition and OAM-SK communication. Using a C-lens to diffract OV_s and extracting characteristic parameters from the diffraction patterns, we can well distinguish OAM modes and improve the discrimination of conjugated modes because the inclined direction of fringes contains the sign information. Since CNN can directly process intensity patterns without pre-processing, it can greatly facilitate the identification and shorten the recognition time. To accurately capture the mode information from diffraction patterns, a six-layer neural network structure consisting of convolution and pooling operations is employed. This design weakens details and emphasizes overall information when extracting the feature information, making the CNN model a certain anti-turbulence ability. The experiment results show that the CNN model can well recognize the OAM modes from -15 to 15 (a total of 30 modes with a mode interval of 1) under the influence of AT, and the accuracies exceed 99% when the turbulence coefficient C_n^2 below $1 \times 10^{-13} \text{ m}^{-2/3}$, $\Delta z = 50 \text{ m}$. Even influenced by the turbulence with $C_n^2 = 1 \times 10^{-12} \text{ m}^{-2/3}$, the accuracy also reaches 89.48%. With an I5-8500 Central Processing Unit (CPU), this identification process only takes 10^{-3} s per OAM mode due to the low time complexity of CNN structure. Furthermore, a Lena gray image with a size of 100×100 pixels was mapped and encoded to different OAM modes to produce OAM-SK signals with 900 modulation orders. After transmission, the signals were demodulated, and the image was well recovered with the turbulence of $C_n^2 = 1 \times 10^{-12} \text{ m}^{-2/3}$. OV_s possess an additional mode freedom with orthogonality, and a certain tolerance to eavesdropping in modulation communication, which make the CNN assisted OAM-SK communication system have great potentials in image encryption transmission, deep space communication, and underwater communication [33].

II. PRINCIPLE

A. THE PREPARATION OF FEATURE EXTRACTION SAMPLES

OV_s can be directly produced by loading spatially helical phase front to Gaussian beams. Its field distribution can be expressed by:

$$E(r, \varphi) = \exp\left(-\frac{r^2}{\omega_0^2}\right) \cdot \exp(il\varphi) \quad (1)$$

where ω_0 represents the waist of the input Gaussian beam.

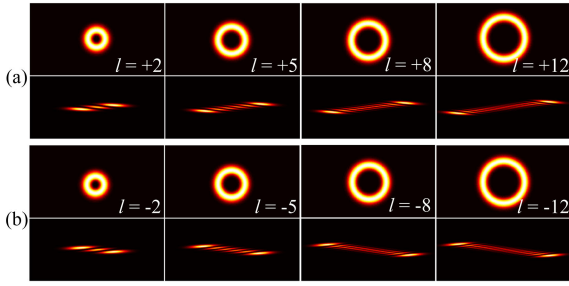


FIGURE 1. The intensity distributions of the OVs with different TCs before and after the C-lens. (a) The OVs with the TCs of $l = +2, +5, +8, +12$. (b) The OVs with the TCs of $l = -2, -5, -8, -12$.

Since the intensity distributions of the OVs with different TCs are similar, especially for the mutual conjugated OVs, it is difficult for CNN to distinguish OAM modes directly from intensity patterns. Here, we use a C-lens to diffract OVs for extracting feature information. Diffraction patterns can directly reflect the sign of OAM modes and have obvious fringes, which help improve the accuracy of recognition. The phase of the C-lens can be described by [34]:

$$\varphi = \exp(-ikx^2/2f), \quad (2)$$

where x is the abscissa in Cartesian coordinates (x, y) , and f is the focal length of the C-lens, $k = 2\pi/\lambda$. After passing through the C-lens, the diffracted intensity patterns of OVs have a stripe shape and contain OAM mode information. As shown in Fig. 1, the number of dark stripes is equal to l , and the oblique direction of the stripes presents the sign of TC. Therefore, using these intensity patterns as the input of CNN, the feature information can be well extracted.

B. THE EFFECTS OF ATMOSPHERIC TURBULENCE

In free-space transmission, AT is one of the most important factors distorting OVs. To explore the influence of turbulences on the OAM mode recognition ability of CNN model, different turbulences are loaded to OVs. In this work, we use a Hill-Andrews model to simulate ATs. The atmospheric refractive index variation spectrum can be written as [35]:

$$\begin{aligned} \Phi_n(k_x, k_y) = & 0.033C_n^2(1 + 1.802\sqrt{\frac{k_x^2 + k_y^2}{k_l^2}} \\ & - 0.254(\frac{k_x^2 + k_y^2}{k_l^2})^{-7/12}) \\ & \cdot \exp(\frac{k_x^2 + k_y^2}{k_l^2})(k_x^2 + k_y^2 + \frac{1}{L_0^2})^{-11/6}, \end{aligned} \quad (3)$$

where k_x and k_y are the frequency wave spectrum data in the x -axis and y -axis directions, respectively. C_n^2 is the refractive index structure constant of AT, which is often used to describe the intensity of ATs, $k_l = 3.3/l_0$, L_0 and l_0 are the outer and inner scale of the turbulence, respectively.

The spectrum variance of the phase screen can be expressed as [36]:

$$\sigma^2(k_x, k_y) = \left(\frac{2\pi}{N\Delta L}\right)^2 \cdot 2\pi k_0^2 \Delta z \Phi_n(k_x, k_y), \quad (4)$$

where ΔL is the grid spacing of the screen. N decides the $N \times N$ phase screen, and Δz is the transmission distance. After fast Fourier transform, the phase screen in spatial frequency domain can be described as [37]:

$$\phi(x, y) = FFT[C_1\sigma(k_x, k_y)], \quad (5)$$

where FFT represents fast Fourier transform, and C_1 is an array of complex random numbers of $N \times N$ dimensions with a mean of 0 and a variance of 1.

Influenced by AT, the amplitude of the beam $U(x, y)$ at the transmission distance of Δz is:

$$U'(x, y) \approx FFT^{-1}[\exp(iA\Delta z) \cdot FFT(\exp(i\phi(x, y)) \cdot U(x, y))], \quad (6)$$

where $\exp(iA\Delta z)$ is the transfer function of Fresnel propagation, $A = (k_x^2 + k_y^2)/(2k)$, and FFT^{-1} represents 2D inverse Fourier transform.

Here, we set the AT phase screen with the size of $N \times N = 512 \times 512$, the grid spacing of $\Delta L = 0.0001$ m, the inner scale of $l_0 = 0.0001$ m, and the outer scale of $L_0 = 50$ m to simulate the influence of ATs on the OAM mode purity, and the simulation results are displayed in Fig. 2. From these figures, the turbulence phase fluctuations are enhanced with the intensity, and the intensity distribution distortion and mode purity reduction of OVs become more serious. This is because the turbulence phase is equivalent to adding a disturbance to the spiral phase, and the degree of disturbance increases with the turbulence intensity. The distorted phase caused by the disturbance will lead to serious mode dispersion and crosstalk, which greatly reduces the purity of the mode. Moreover, the degree of phase distortion is also related to OAM modes. The larger the TC is, the larger the proportion of the information determining the mode in the phase, which leads to a greater influence of AT. The simulation results are shown in Fig. 3. From the figure, influenced by the same AT, the mode purity of OVs decreases with the increase of TC, and the mode purity of the OV with large TCs has a 5% decline compared with the small one. As the turbulence intensity increases from $C_n^2 = 1 \times 10^{-13} \text{ m}^{-2/3}$ to $C_n^2 = 1 \times 10^{-12} \text{ m}^{-2/3}$, the mode purities of the OVs with $l = 1, 2, \text{ and } 3$ are reduced by about 40%. In the recognition, this degeneration will directly distort the intensity distribution and make the OAM mode information hard to be extracted, which may result in a great decrease in identification accuracy.

C. THE CNN MODEL FOR OAM MODES RECOGNITION

Compared with other neural networks, CNN has a feature extractor comprising convolutional and subsampling layers, which is suitable for image recognition and classification.

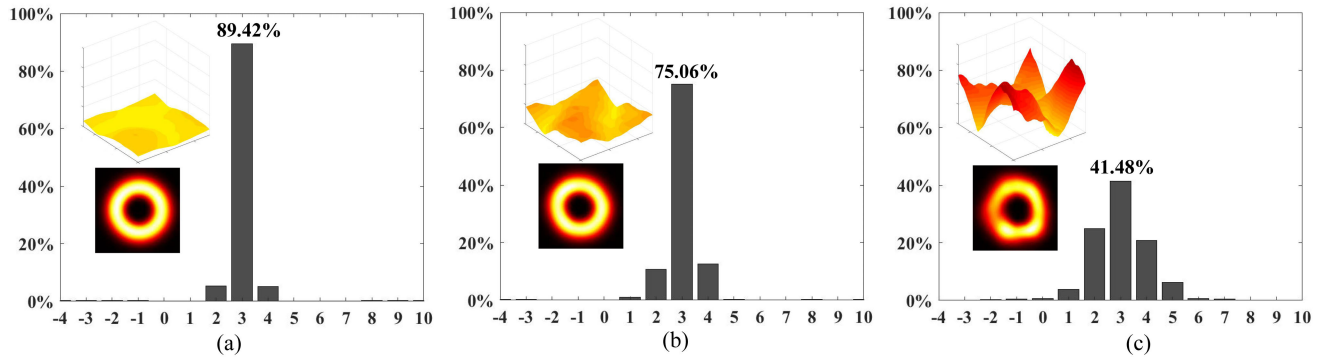


FIGURE 2. The mode purity and phase distribution of the OV ($l = +3$) under the influence of different ATs at $\Delta z = 50$ m. (a) $C_n^2 = 1 \times 10^{-14} \text{ m}^{-2/3}$; (b) $C_n^2 = 1 \times 10^{-13} \text{ m}^{-2/3}$; (c) $C_n^2 = 1 \times 10^{-12} \text{ m}^{-2/3}$.

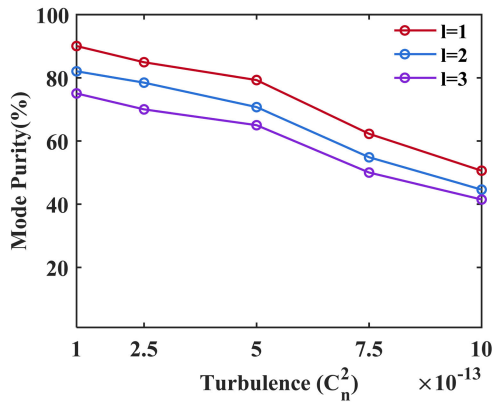


FIGURE 3. The mode purity of OVs under the influence of different ATs.

In this work, we have designed a CNN model with strong image processing capability to identify the OAM mode of OVs. Since CNN can directly extract and classify feature information by learning input light intensity patterns, it avoids the complex and time-consuming step of extracting the explicit features of OAM modes.

The convolutional layer, in which a neuron connects a part of neurons in the previous layer, detect the local features of input images. The local connection will greatly reduce the number of parameters and speed up the learning. In general, a convolutional layer contains multiple convolution kernels, and the neurons in the same convolution kernel share the weights, which can help reduce the connections between layers and the risk of overfitting. Different feature images can be extracted by applying different convolution kernels onto the output of the previous layer, and taken as the input of next layers. Each element of the feature image in a convolutional layer can be expressed as [38]:

$$y_j^p = f \left(b_j^p + \sum_{i \in M_j} x_i^{p-1} * k_{ij}^p \right), \quad (7)$$

where M_j represents a group of feature images in the $(p - 1)^{th}$ layer. The input x_i^{p-1} and corresponding output y_j^p denote the i^{th} and j^{th} feature image in the $(p - 1)^{th}$ and p^{th} layer, respectively. k_{ij}^p is the convolution kernel associated with

x_i^{p-1} and y_j^p . The symbol $*$, b_j^p and f represent the convolution operation, bias term, and nonlinear activation function, respectively. To further reduce the dimension of feature images and network parameters, the convolutional layer is usually followed by a pooling layer. After rounds of convolution and pooling, a set of implicit features are learned from the original input image. To map the achieved image features to desired outputs, the end of the CNN is often followed by several fully connected layers, and a *softmax* or *regression* layer.

The proposed CNN architecture is shown in Fig. 4 and consists of six layers. The first to fourth layers are convolutional layers, and the last two layers are full-connection and output layers. The input images are the grayscale intensity patterns of the OVs diffracted by C-lens, and each image is resized to 128×128 pixels. The first convolutional layer employs 5×5 convolution kernels, the second to fourth layers employ 3×3 convolution kernels, and each layer is followed by a maximum pooling layer. The activation function used for each convolutional layer is Rectified Linear Units (*ReLU*, $ReLU(x) = \max(x, 0)$), and the input images with a size of 128×128 are mapped to feature images of 16×16 pixels after convolutional and max-pooling layers. Finally, a fully connected layer and a *softmax* classifier are applied to transfer the feature images to desired outputs. Dropout is used in the fully connected layer to reduce overfitting. The mathematical expression of the *softmax* function is [39]:

$$f(x_i, \theta) = softmax(z_i) = \frac{\exp(z_i)}{\sum_j \exp(z_j)}, \quad (8)$$

where z_i represents the output of the i^{th} neuron, j represents the number of categories of the final output. The output result of the *softmax* function is $f(x_i, \theta)$, which can be trained to approximate the actual Y by minimizing the cross-entropy loss function [40]:

$$L(f(X, \theta), Y) = - \sum y_i \ln f(x_i, \theta). \quad (9)$$

III. EXPERIMENTAL RESULTS AND ANALYSIS

Figure 5 presents the schematic diagram of identifying OAM modes by using the CNN model. Turning the angle of the

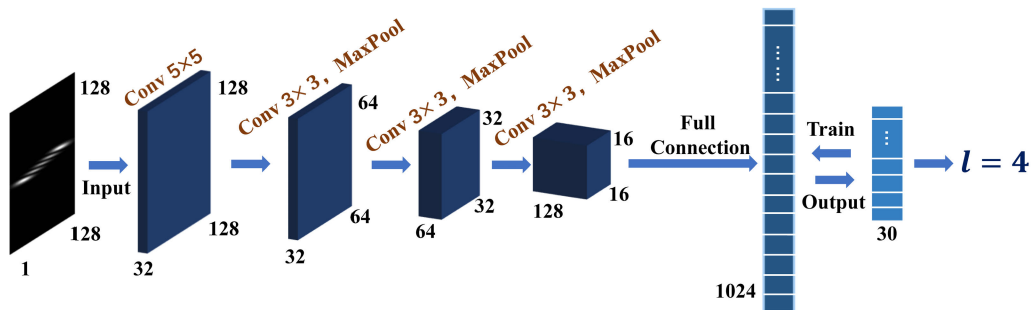


FIGURE 4. The architecture of the CNN model. Conv: convolution.

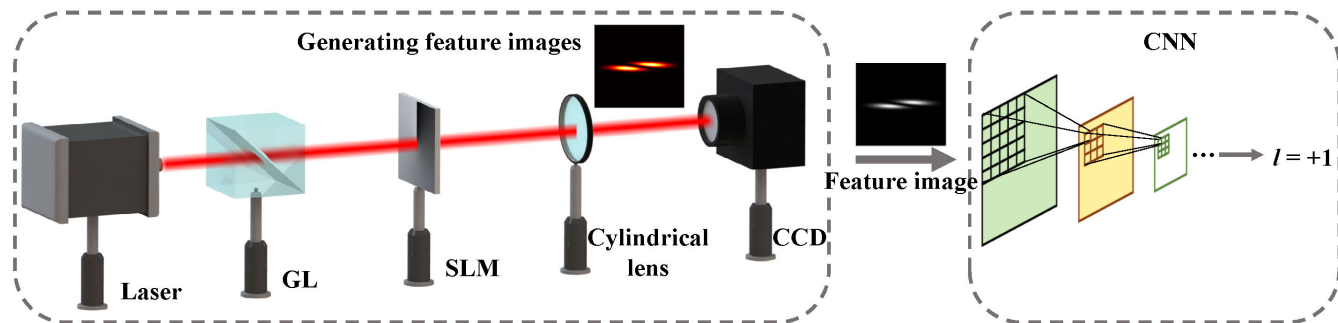


FIGURE 5. The schematic diagram of the generation and acquisition of input images for the CNN. GL: Glan prism; SLM: Spatial light modulator; CCD: Charge coupled device.

TABLE 1. Parameters of the experimental system.

Parameters	Values
Waist of the incident Gauss beam	1 mm
Sensor area of SLM	8.64 mm*15.36 mm
Pixels of SLM	1080*1920
Focal length of the C-lens	100 mm
OAM channel length	50 cm
Maximum FSO link length	1.1 m
Frame rate of CCD	17 fps
The radius of OV with $l=1$	1 mm
The radius of OV with $l=15$	3.25 mm

Glan prism to 0° , the horizontally polarized Gauss beam was converted into OVs by the spatial light modulator loaded with spiral phases. The OAM mode of the OV can be regulated by the loaded spiral phases. Because the OV has a “doughnut” intensity distribution, the characteristics of different OAM modes are less apparent. To extract the feature information more conveniently, a C-lens was employed to diffract OVs and generate stripe formed feature images related to TCs. By training a large number of such stripe-shaped diffraction patterns, the CNN model can well identify OAM modes.

In this work, a He-Ne laser was used as light source, the parameters of the experiment system are shown in Table 1, and the size and grid spacing of the turbulence screen are set in accordance with the SLM parameters. We first loaded the AT with different turbulence phase distributions on 30 OVs, where $C_n^2 = 1 \times 10^{-14} \text{ m}^{-2/3}$, $\Delta z = 50 \text{ m}$. And in the experiment, we only use one SLM to generate OAM

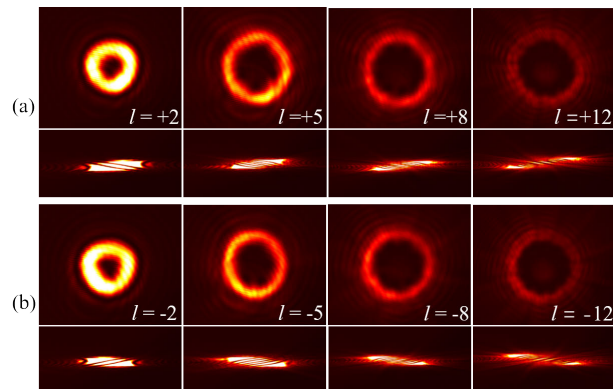


FIGURE 6. The intensity distributions of the OVs with different TCs before and after the C-lens under the influence of $C_n^2 = 1 \times 10^{-14} \text{ m}^{-2/3}$.

modes and emulate the turbulence phase distortion. Figure 6 displays the intensity distributions of the OVs with $l = \pm 2, \pm 5 \pm 8, \pm 12$ before and after the C-lens. From the figures, even influenced by weak turbulence, the OVs with high-order OAM modes (such as $l = +8$) are difficult to be recognized. In the experiment, we randomly generated 6000 phase images with TCs within the interval of $[-15, 15]$ and added the turbulence of $C_n^2 = 1 \times 10^{-14} \text{ m}^{-2/3}$ on the phases. The intensity diffraction patterns of the OVs passing through the C-lens were collected. Among them, 4000 grayscale images were used as training inputs for the CNN, and the remaining 2000 grayscale images were used as test data.

During the training, the Adam optimization function provided by TensorFlow is used to minimize the loss value,

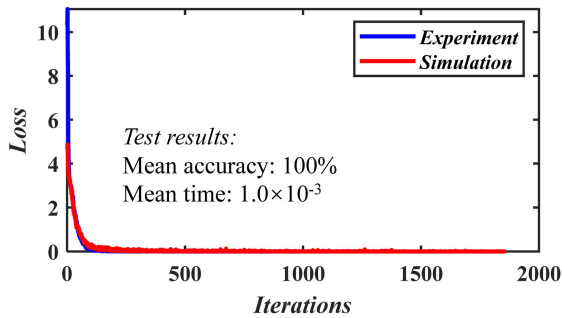


FIGURE 7. The loss function curve and test results under the influence of $C_n^2 = 1 \times 10^{-14} \text{ m}^{-2/3}$.

and the learnable parameters in the network are dynamically adjusted to achieve the best fitting. And there is an expected decrease in loss value with the increase of iterations (see the blue line in Fig.7). When the iteration increased to 200, the loss value is almost close to 0, which demonstrates that the CNN model has established a good mapping relationship between the input and the ideal output. However, the training loss value cannot completely evaluate the performance of CNNs. The test accuracy representing the generalization ability is another important evaluating criteria. Here, we used 2000 images to test the trained CNN model, the results show that the mean accuracy is 100%, and the mean time required for testing one pattern takes only 1.0×10^{-3} s by using an I5-8500 CPU, indicating that the CNN model can accurately and quickly identify OAM modes under the influence of AT with $C_n^2 = 1 \times 10^{-14} \text{ m}^{-2/3}$. Besides, we have simulated the whole experimental system, the system parameters are consistent with the experiment. The training results are shown by the red line in Fig. 7, which is coincident with the loss function curve in the experimental results, and the test accuracy is also 100%. It shows that the experimental results are consistent with the simulations.

The reason why CNN can identify OAM mode with 100% accuracy is that ATs with $C_n^2 = 1 \times 10^{-14} \text{ m}^{-2/3}$ have a weaker effect on the spiral phase, and the distortion randomness of the phase and intensity distribution are small, which make the input diffraction patterns belonging to the same OAM mode category maintain strong similarity. Therefore, CNN can accurately capture the feature information.

To further test the applicability of the CNN model to environments, we increased the turbulence to $C_n^2 = 1 \times 10^{-13} \text{ m}^{-2/3}$ with $\Delta z = 50$ m. As depicted in Fig. 8, the intensity distributions of OVVs begin to distort, and the diffraction patterns are also deformed. The training and testing results are shown in Fig. 9. When the training iterations reach 500, the loss function tends to be stable and reaches around 0. Using the trained CNN model for testing, the average accuracy reaches 99.43%, and the average time consumption is only 1.0×10^{-3} s. Compared with the case of $C_n^2 = 1 \times 10^{-14} \text{ m}^{-2/3}$, it needs more iterations to reduce the loss value to 0, and the testing accuracy also decreases. This is because the increase of turbulence intensity will cause an enhanced distortion on the light intensity distribution,

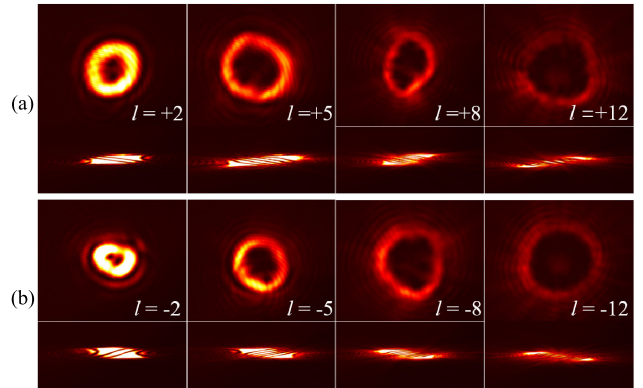


FIGURE 8. The intensity distributions of OVVs before and after the C-lens under the influence of $C_n^2 = 1 \times 10^{-13} \text{ m}^{-2/3}$.

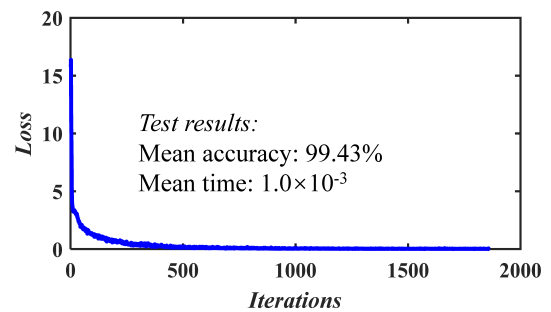


FIGURE 9. The loss function curves and test results under the influence of $C_n^2 = 1 \times 10^{-13} \text{ m}^{-2/3}$.

which will result in the reduction of effective information and brings a certain degree of interference to the information extraction. However, the time consumption has not been improved because the time complexity of the CNN model is determined by the network structure, and both adopted model structures are the same structure in Fig. 5.

From the previous analysis, under the influence of the turbulences with $C_n^2 = 1 \times 10^{-13} \text{ m}^{-2/3}$ or $C_n^2 = 1 \times 10^{-14} \text{ m}^{-2/3}$, the proposed CNN structure can well identify OAM modes, and the average accuracy exceeds 99%. In practical applications, environmental factors are more complicated, and stronger turbulences are often difficult to avoid. Therefore, we increased the AT to $C_n^2 = 1 \times 10^{-12} \text{ m}^{-2/3}$ with $\Delta z = 50$ m. As shown in Fig. 10, the stronger AT has a large phase fluctuation, which causes severe distortions in the phase and intensity distribution of OVVs, and the diffraction patterns become very messy. Even for the OVVs with low-orders, it is difficult to distinguish. However, with the excellent implicit feature information capture capability, the CNN can also obtain the OAM mode information even if the OVVs are severely distorted. Figure 11 demonstrates the loss function as the function of iterations. The loss function can also be reduced to about 0 at the 1500th iteration. And the average accuracy of the test reaches 89.48%. It takes only 1.0×10^{-3} s for identifying one test image. The reason why the test accuracy is greatly reduced is that the turbulence phases used in the training and test sets are not shared. The stronger turbulence causes more random distortion in the intensity distribution, which

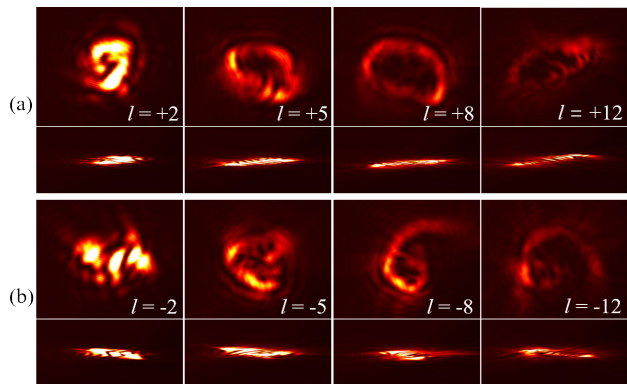


FIGURE 10. The intensity distributions of OVs before and after the C-lens under the influence of $C_n^2 = 1 \times 10^{-12} \text{ m}^{-2/3}$.

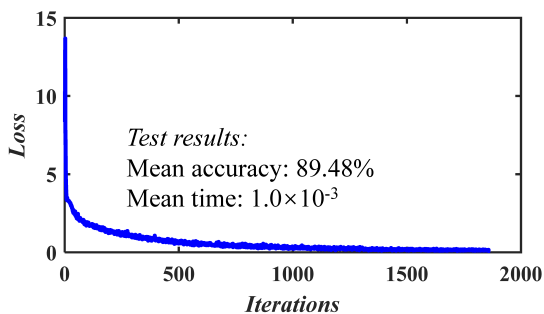


FIGURE 11. The loss function curves and test results under the influence of $C_n^2 = 1 \times 10^{-12} \text{ m}^{-2/3}$.

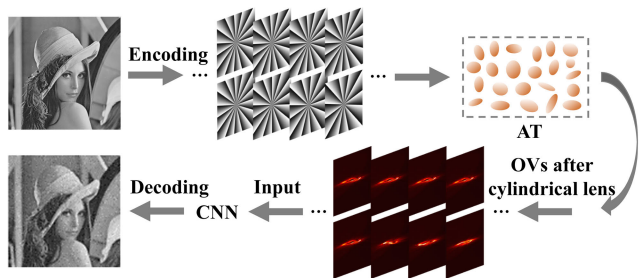


FIGURE 12. The diagram of the CNN-based communication link for transmitting a 100×100 pixels Lena gray image.

severely reduces the similarity of the diffraction pattern data belonging to the same OAM mode category, and increases the difficulty of CNN to capture valid mode information. However, the characteristics of local connection reduce the sensitivity of CNN to the global change of the objects. Thus, the test accuracy can still reach 89.48%, which also indicates that our proposed CNN model has a good generalization ability.

In the above, we have used the CNN to train and test the OAM mode datasets affected by three different intensities of AT, and the corresponding CNN models with great OAM mode recognition ability are obtained. It is worth noting that these three data sets are trained and tested by the same CNN simulation model, which is shown in Fig. 5.

Due to the unique spiral phase structure and orthogonality, OVs are often used in communications to increase communication capacity and modulation ability. Thus, we constructed

an OAM-SK communication link to encode images and used this CNN model to decode OAM-SK signals. As illustrated in Fig. 12, a Lena gray image with a size of 100×100 pixels was encoded into two OAM-SK channels, and each pixel value corresponds to two OAM modes. Mapping pixel values ranging from 0 to 255 to two bits numbers with non-zero values, each bit representing an OAM mode whose value is equal to the TC, and the high and low bits are represented by l_1 and l_2 , respectively. The value of each bit is 30-ary, and the minimum is -15 . Specifically, the gray value 0 corresponds to two OAM modes with the smallest TC ($l_1 = -15$, $l_2 = -15$), and the gray value 1 increases by 1 at the low bit of the gray value 0 ($l_1 = -15$, $l_2 = -14$). Following this law, we have obtained 20000 spiral phase images, which were sequentially transmitted through ATs with $C_n^2 = 1 \times 10^{-12} \text{ m}^{-2/3}$. Then, the stripe feature patterns diffracted by the C-lens were inputted into the previously trained CNN model, and the TCs predicted by CNN were decoded in the opposite way to the encoding. Finally, a complete restored Lena gray image was obtained. It should be noted that two OAM channels are used here and each channel has 30 OAM modes ($l \in [-15, 15]$), which indicates that the modulation capability of the proposed OAM-SK communication link reaches 900-order.

It can be seen that the restored Lena grayscale image is almost the same as the original image, which demonstrates that even under the influence of turbulence with $C_n^2 = 1 \times 10^{-12} \text{ m}^{-2/3}$, the CNN can still recognize OAM modes well. This illustrates that the CNN assisted OAM modes recognition method we proposed has a good generalization ability and adaptability to different environments.

In the experiment, the communication capability of OAM-SK systems is limited by the response speed of SLM and CCD. Here, the SLM and CCD operated at ~ 50 Hz, and the response times are around 0.1 s and 0.058 s, respectively, which limit the symbol rate of the OAM-SK communication system to about 10 baud/s. However, other devices with faster response speed can be used to effectively increase the communication capability, such as digital micro-mirror device (DMD) and complementary metal-oxide-semiconductor (CMOS) with operating frequency up to kilohertz and response time down to milliseconds, which can increase the symbol rate by nearly ten times.

IV. DISCUSSION

Here, we propose a CNN-assisted OAM pattern recognition method, which can be used in OAM optical communication and quantum signal processing, etc. The OVs are diffracted by a C-lens for feature extraction, and the OAM modes are recognized from the diffraction patterns by CNN. Firstly, we analyze the feature patterns obtained by C-lens diffraction, and the recognition of OAM modes with CNN will be discussed in detail later. The C-lens is mainly used to make the OAM mode feature information more obvious, which can also be realized by interference methods, such as interfering the OVs with a plane wave or a spherical wave and

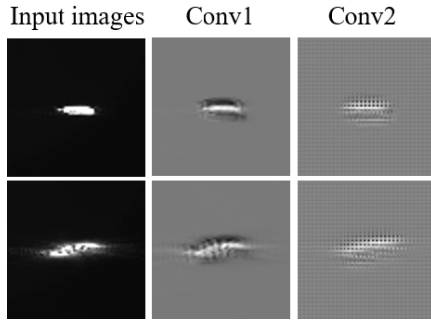


FIGURE 13. Input images of the CNN, and features captured by the convolutional layers.

obtaining the interference patterns containing OAM mode information. However, to satisfy the coherent condition, it is necessary to find a coherent beam for the interfering that is difficult in practical applications. In addition, the C-lens has the advantages of small size, easy operation, and flexibility. Therefore, the use of C-lens diffraction is more suitable. But this method also has some defects. For example, the features of the OV_s with large TC_s are not obvious. Especially under the influence of turbulence, the effective information that can be captured by CNN is limited, which limits the detection of the OAM mode with larger TC_s. Besides, the C-lens diffraction method is only suitable for the identification of single OAM modes. For the hybrid OAM modes, effective feature diffraction patterns cannot be obtained on the focal plane of C-lens, which may be solved by using a Dammann grating combined with a feedforward neural network.

The main function of convolutional layers in the CNN is to capture the effective information from input images, and the more layers there are, the more accurate the captured information will be. The whole network spreads forward, and the information is processed step by step. The low layers capture the basic features that are integrated by the high layers. And the information processed by the high-layer is more abstract. The size of the collected light intensity distribution images is 840×600 . To reduce the time complexity of the whole neural network, they are reshaped into 128×128 and inputted into the CNN model. The pixel of images is reduced by almost 5 times, resulting in some details of the intensity distribution to be lost. The proposed CNN architecture is built with TensorFlow, and the input image and features captured by each convolutional layer can be visualized by TensorBoard (see Fig. 13). Taking the training input images of $l = 1$ and $l = 4$ under the influence of $C_n^2 = 1 \times 10^{-13} \text{ m}^{-2/3}$ as examples, after 60 training epochs, the first convolutional layer predicts the location of valid information and extracts some edge information. The second convolutional layer performs feature extraction based on the first layer. Since the maximum pooling is done after convolution, the size of the image is reduced, resulting in the blurring of featured images. The details have been abstracted, and the more pooling, the more abstract the feature map will be. The CNN extracts the OAM mode information from the overall shape of light intensity

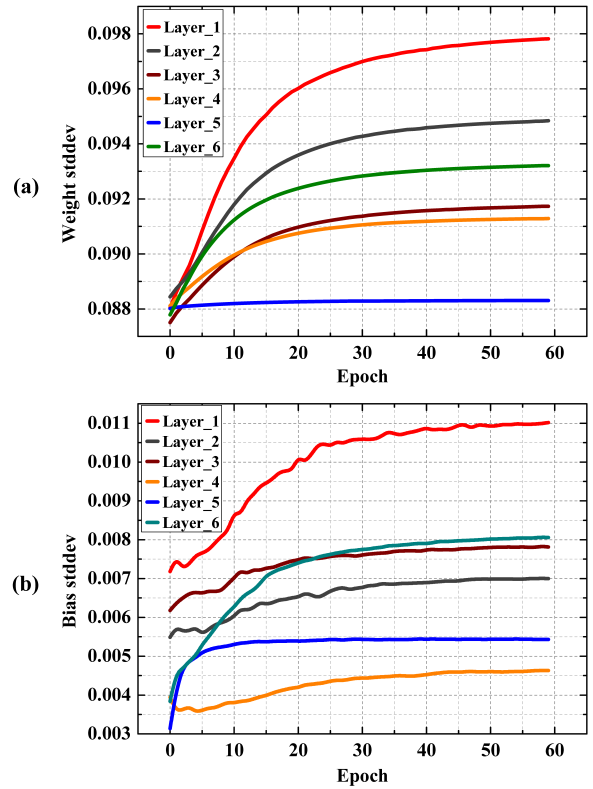


FIGURE 14. The weight and bias stddev curves as the function of training epoch.

distributions. Even influenced by turbulence, the light intensity distributions of different OAM modes are still different, which makes CNN has a certain anti-interference ability.

The deep neural network is mainly optimized by continuously updating the weights and biases during the training process. As the training period increases, the maximum values of weights and biases increase, and the minimum value tends to be smaller. At the same time, the variance becomes larger, which is an ideal state that each neuron should pay attention to different characteristics and results in a large difference between parameters. Figure 14 shows the trend of weight and bias stddev in the training process for extracting the OAM mode information influenced by the turbulence of $C_n^2 = 1 \times 10^{-13} \text{ m}^{-2/3}$ and the weight refers to the convolution kernel in the convolutional layer. As the training epoch increases from 0 to 60, the weights and bias stddev of six layers have an upward trend, of which the weight stddev of the first layer increases from 0.088052 to 0.097822. This indicates that each layer of the trained CNN structures has a clear division of labor, which makes the CNN model a good OAM mode information extraction ability.

When training the CNN model, selecting enough training data is an effective method to improve generalization abilities. In addition, a large and diverse training data can effectively prevent overfitting. Here, we collected 4000 samples as the training set, and the recognition accuracy with the turbulence intensity of $C_n^2 = 1 \times 10^{-13} \text{ m}^{-2/3}$ reaches 99.43%. To study the impact of the size of training data on the

TABLE 2. The mean test accuracy for different numbers of training data.

The number of training data	Mean test accuracy
1000	0.8724
2000	0.9620
3000	0.9911
4000	0.9943

TABLE 3. The mean test accuracy for different CNN structures.

The number of training layers	Mean test accuracy	Mean time
4	0.9724	9.9265e-04
5	0.9849	9.9901e-04
6	0.9943	1.0e-03

TABLE 4. The mean test accuracy for different distances.

Distance (m)	Mean test accuracy
10	0.9984
50	0.9943
100	0.9694
200	0.9568

performance, we selected 1000, 2000, 3000 and 4000 training data to train the CNN model, and the corresponding mean test accuracies are shown in Table 2. From the comparison results, the mean test accuracy increases with the training data. Besides, we have studied the prediction ability of the CNN model corresponding to different numbers of convolution layer. 4000 samples are trained using 4, 5, and 6 layers, respectively. Then, the mean accuracies of the CNN model and the times required to identify an OAM mode are tested (see Table 3). From the results, the recognition accuracy of the 4-layer structure is reduced to 97.24%, which is because more effective information can be captured by appropriately increasing the number of training layers. Meanwhile, the time required for the 4-layer network to recognize OAM modes is minimal. The calculation time of CNN is not only related to computer performances, but also depends on the time complexity of the CNN model, and the time complexity is related to the complexity of networks. The more layers are, the more average time is required to identify an OAM mode.

In addition to the above factors, the AT transmission distance will also affect the accuracy of recognition. In the case of fixed turbulence intensity, the longer the transmission distance is, the greater the disturbance of OAM mode is accumulated. And the worsened phase distortions directly increase the noise in the diffraction patterns and reduce the recognition accuracy of CNN. Comparing $\Delta z = 10$ m, 100 m, and 200 m with $\Delta z = 50$ m, $C_n^2 = 1 \times 10^{-13} \text{ m}^{-2/3}$, the experimental results (see Table 4) show that as the distance increases from $\Delta z = 10$ m to $\Delta z = 200$ m, the mean test accuracy decreased from 0.9984 to 0.9568, which further proves that the OAM mode is more seriously affected with the distance.

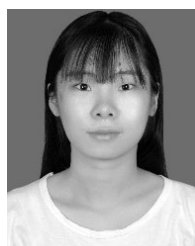
V. CONCLUSION

In conclusion, we proposed and experimentally demonstrated a CNN-assisted method for OAM modes recognition and communication. A C-lens was used to diffract OV to form a striped light intensity distribution associated with OAM mode. Training the CNN model with a large number of diffraction grayscale images, it was succeeded in quickly identifying OAM modes ranging from -15 to $+15$. The experimental results show that the trained CNN model has a good recognition ability in different AT environments. The accuracies exceed 99% with $C_n^2 = 1 \times 10^{-13} \text{ m}^{-2/3}$ and $C_n^2 = 1 \times 10^{-14} \text{ m}^{-2/3}$, and the detection accuracy of 89.48% is also achieved influenced by the turbulence of $C_n^2 = 1 \times 10^{-12} \text{ m}^{-2/3}$. To further investigate the recognition performance of the CNN model and its potential in communications, an OAM-SK communication system was constructed. And a Lena gray image of 100×100 pixels was mapped and encoded to two OAM channels which have 900-order modulation ability to form OAM-SK signals. After transmission in the AT with $C_n^2 = 1 \times 10^{-12} \text{ m}^{-2/3}$, the OAM information included in the intensity patterns diffracted by the C-lens was predicted by the CNN model, and the image was well restored, which may show great potentials in optical communication and quantum communication, etc.

REFERENCES

- [1] A. M. Yao and M. J. Padgett, "Orbital angular momentum: Origins, behavior and applications," *Adv. Opt. Photon.*, vol. 3, no. 2, pp. 161–204, Jun. 2011.
- [2] J. Verbeeck, H. Tian, and P. Schattschneider, "Production and application of electron vortex beams," *Nature*, vol. 467, no. 7313, pp. 301–304, 2010.
- [3] M. Su, J. Liu, Y. He, S. Chen, and Y. Li, "Optical orbital angular momentum demultiplexing and channel equalization by using equalizing dammann vortex grating," *Adv. Condens. Matter Phys.*, vol. 2017, Jun. 2017, Art. no. 6293910.
- [4] Y. He, L. Ying, J. Liu, X. Zhang, C. Yao, C. Yu, S. Chen, and D. Fan, "Switchable phase and polarization singular beams generation using dielectric metasurfaces," *Sci. Rep.*, vol. 7, no. 1, 2017, Art. no. 6814.
- [5] J. Liu, P. Wang, Y. He, X. Zhou, J. Xiao, Y. Li, S. Chen, and S. Xu, "Modes coded modulation of vector light beams using spatial phase cross-polarized modulation," *Opt. Commun.*, vol. 432, pp. 59–64, Feb. 2019.
- [6] L. Allen, S. M. Barnett, and M. J. Padgett, *Optical Angular Momentum*. Boca Raton, FL, USA: CRC Press, 2016, pp. 109–186.
- [7] K. Dholakia and T. Čížmár, "Shaping the future of manipulation," *Nature Photon.*, vol. 5, no. 6, pp. 335–342, 2011.
- [8] N. Eeckerskorn, R. Bowman, R. A. Kirian, S. Awel, M. Wiedorn, J. Küpper, M. J. Padgett, H. N. Chapman, and A. V. Rode, "Optically induced forces imposed in an optical funnel on a stream of particles in air or vacuum," *Phys. Rev. Appl.*, vol. 4, no. 6, 2015, Art. no. 064001.
- [9] D. G. Grier, "A revolution in optical manipulation," *Nature*, vol. 424, no. 6950, pp. 810–816, Aug. 2003.
- [10] X. Zhang, Y. He, Y. Cai, M. Su, X. Zhou, Y. Chen, S. Chen, Y. Xiang, L. Chen, Y. Li, D. Fan, and C. Su, "Coherent separation detection for orbital angular momentum multiplexing in free-space optical communications," *IEEE Photon. J.*, vol. 9, no. 3, Jun. 2017, Art. no. 7903811.
- [11] H. Wu, J. Tang, Z. Yu, J. Yi, S. Chen, J. Xiao, C. Zhao, Y. Li, L. Chen, and S. Wen, "Electrically optical phase controlling for millimeter wave orbital angular momentum multi-modulation communication," *Opt. Commun.*, vol. 393, pp. 49–55, Jun. 2017.
- [12] A. Mair, A. Vaziri, G. Weihs, and A. Zeilinger, "Entanglement of the orbital angular momentum states of photons," *Nature*, vol. 412, no. 6844, pp. 313–316, Jul. 2001.

- [13] Y. He, Y. Li, Y. Cai, X. Zhang, J. Liu, J. Xiao, S. Chen, and D. Fan, "A full-duplex 100-GHz radio-over-fiber communication system based on frequency quadrupling," *Optik*, vol. 175, pp. 148–153, Dec. 2018.
- [14] J. Wang, J.-Y. Yang, I. M. Fazal, N. Ahmed, Y. Yan, H. Huang, Y. Ren, Y. Yue, S. Dolinar, A. E. Willner, and M. Tur, "Terabit free-space data transmission employing orbital angular momentum multiplexing," *Nature Photon.*, vol. 6, no. 7, p. 488–496, Jul. 2012.
- [15] B. Nenad, Y. Yang, R. Yongxiong, T. Moshe, K. Poul, H. Hao, W. Alan E, and R. Siddharth, "Terabit-scale orbital angular momentum mode division multiplexing in fibers," *Science*, vol. 340, no. 6140, pp. 1545–1548, Jun. 2013.
- [16] M. Harris, C. A. Hill, P. R. Tapster, and J. M. Vaughan, "Laser modes with helical wave fronts," *Phys. Rev. A, Gen. Phys.*, vol. 49, no. 4, p. 3119, 1994.
- [17] M. S. Soskin, V. N. Gorshkov, M. V. Vasnetsov, J. T. Malos, and N. R. Heckenberg, "Topological charge and angular momentum of light beams carrying optical vortices," *Phys. Rev. A, Gen. Phys.*, vol. 56, no. 5, pp. 4064–4075, 1997.
- [18] N. Zhang, X. C. Yuan, and R. E. Burge, "Extending the detection range of optical vortices by Dammann vortex gratings," *Opt. Lett.*, vol. 35, no. 20, pp. 3495–3497, 2010.
- [19] S. Fu, T. Wang, S. Zhang, and C. Gao, "Integrating 5×5 Dammann gratings to detect orbital angular momentum states of beams with the range of -24 to $+24$," *Appl. Opt.*, vol. 55, no. 7, pp. 1514–1517, 2016.
- [20] M. E. Anderson, H. Bigman, L. E. E. De Araujo, and J. L. Chaloupka, "Measuring the topological charge of ultrabroadband, optical-vortex beams with a triangular aperture," *J. Opt. Soc. Amer. B, Opt. Phys.*, vol. 29, no. 8, pp. 1968–1976, 2012.
- [21] G. Cheng-Shan, L. Lei-Lei, and W. Hui-Tian, "Characterizing topological charge of optical vortices by using an annular aperture," *Opt. Lett.*, vol. 34, no. 23, pp. 3686–3688, 2009.
- [22] D. Vladimir, S. Vladlen, A. S. Desyatnikov, D. N. Neshev, K. Wieslaw, V. Alexander, S. Marat, and Y. S. Kivshar, "Determination of topological charges of polychromatic optical vortices," *Opt. Express*, vol. 17, no. 26, pp. 23374–23379, 2009.
- [23] M. J. Padgett and L. Allen, "Orbital angular momentum exchange in cylindrical-lens mode converters," *J. Opt. B, Quantum Semiclass. Opt.*, vol. 4, no. 2, p. S17, 2002.
- [24] I. J. Goodfellow, Y. Bulatov, J. Ibarz, S. Arnaud, and V. Shet, "Multi-digit number recognition from street view imagery using deep convolutional neural networks," 2014, *arXiv:1312.6082*. [Online]. Available: <https://arxiv.org/abs/1312.6082>
- [25] J. Gu, Z. Wang, J. Kuen, L. Ma, A. Shahroudy, B. Shuai, T. Liu, X. Wang, L. Wang, J. Cai, T. Chen, and G. Wang, "Recent advances in convolutional neural networks," 2015, *arXiv:1512.07108*. [Online]. Available: <https://arxiv.org/abs/1512.07108>
- [26] N. Kalchbrenner, L. Espeholt, K. Simonyan, A. Van Den Oord, A. Graves, and K. Kavukcuoglu, "Neural machine translation in linear time," 2016, *arXiv:1610.10099*. [Online]. Available: <https://arxiv.org/abs/1610.10099>
- [27] S. Lohani and R. T. Glasser, "Turbulence correction with artificial neural networks," *Opt. Lett.*, vol. 43, no. 11, pp. 2611–2614, 2018.
- [28] S. Lohani, E. M. Knutson, and M. O'Donnell, S. D. Huver, and R. T. Glasser, "On the use of deep neural networks in optical communications," *Appl. Opt.*, vol. 57, no. 15, pp. 4180–4190, 2018.
- [29] A. Dikopoltsev, D. Moss, G. I. Haham, M. Segev, O. Cohen, S. Mannor, and T. Zahavy, "Deep learning reconstruction of ultrashort pulses," *Optica*, vol. 5, no. 5, pp. 666–673, 2018.
- [30] T. Doster and A. T. Watnik, "Machine learning approach to OAM beam demultiplexing via convolutional neural networks," *Appl. Opt.*, vol. 56, no. 12, pp. 3386–3396, 2017.
- [31] E. M. Knutson, S. Lohani, O. Danaci, S. D. Huver, and R. T. Glasser, "Deep learning as a tool to distinguish between high orbital angular momentum optical modes," *Proc. SPIE*, vol. 9970, Sep. 2016, Art. no. 997013.
- [32] J. Li, M. Zhang, D. Wang, S. Wu, and Y. Zhan, "Joint atmospheric turbulence detection and adaptive demodulation technique using the CNN for the OAM-FSO communication," *Opt. Express*, vol. 26, no. 8, pp. 10494–10508, 2018.
- [33] Q. Tian, Z. Li, K. Hu, L. Zhu, X. Pan, Q. Zhang, Y. Wang, F. Tian, X. Yin, and X. Xin, "Turbo-coded 16-ary OAM shift keying FSO communication system combining the CNN-based adaptive demodulator," *Opt. Express*, vol. 26, no. 21, pp. 27849–27864, 2018.
- [34] X. Fang, Z. Kuang, P. Chen, H. Yang, Q. Li, W. Hu, Y. Lu, Y. Zhang, and M. Xiao, "Examining second-harmonic generation of high-order Laguerre–Gaussian modes through a single cylindrical lens," *Opt. Lett.*, vol. 42, no. 21, pp. 4387–4390, 2017.
- [35] L. C. Andrews, "An analytical model for the refractive index power spectrum and its application to optical scintillations in the atmosphere," *J. Mod. Opt.*, vol. 39, no. 9, pp. 1849–1853, 1992.
- [36] S. Zhao, J. Leach, and B. Zheng, "Aberration corrections for free-space optical communications in atmosphere turbulence using orbital angular momentum states," *Opt. Express*, vol. 20, no. 1, pp. 452–461, Jan. 2012.
- [37] J. D. Strasburg and W. W. Harper, "Impact of atmospheric turbulence on beam propagation," *Proc. SPIE*, vol. 5413, pp. 93–102, Sep. 2004.
- [38] P. Wang and J. Di, "Deep learning-based object classification through multimode fiber via a CNN-architecture SpeckleNet," *Appl. Opt.*, vol. 57, no. 28, pp. 8258–8263, 2018.
- [39] R. A. Dunne and N. A. Campbell, "On the pairing of the softmax activation and cross-entropy penalty functions and the derivation of the softmax activation function," in *Proc. 8th Aust. Conf. Neural Netw.*, vol. 181, Jun. 1997, p. 185.
- [40] J. Liu, W. C. Chang, Y. Wu, and Y. Yang, "Deep learning for extreme multi-label text classification," in *Proc. 40th Int. ACM SIGIR Conf. Res. Develop. Inf. Retr.*, Aug. 2017, pp. 115–124.



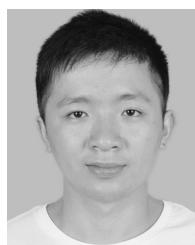
PEIPEI WANG received the B.E. degree from the Hunan Institute of Science and Technology, China, in 2017. She is currently pursuing the master's degree with the Physics and Optoelectronic Engineering College, Shenzhen University. Her main research interests include intelligent information processing and optical communication based on structured beam.



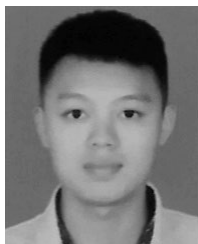
JUNMIN LIU received the B.S. and M.E. degree in computer science and technology from Hunan University, China, in 2010 and 2013, respectively, and the Ph.D. degree from Shenzhen University, China, in 2019. She is currently a Researcher with the College of New Materials and New Energies, Shenzhen Technology University. Her main research interests include intelligent information processing and optical communication.



LIJUAN SHENG received the B.S. degree in physics from Gannan Normal University, China, in 2017. She is currently pursuing the master's degree in electronic science and technology with Hunan Normal University. Her research interest includes applications of photonic spin Hall effect. She has received the National Scholarship of Graduate Students, in 2018.



YANLIANG HE received the B.S. degree in optical information science and technology from East China Jiaotong University, China, in 2015. He is currently pursuing the Ph.D. degree with the Physics and Optoelectronic Engineering College, Shenzhen University. His main research interest includes structured light field regulation.



WENJIE XIONG received the B.S. degree in electronic science and technology from the Hunan Institute of Technology, in 2018. He is currently pursuing the master's degree with the Physics and Optical Engineering College, Shenzhen University. His main research interests include intelligent information processing and optical communication based on structured beams.



SHUQING CHEN received the Ph.D. degree from Hunan University, China, in 2015. In September 2015, he joined the 2D Materials Optoelectronic Technology International Cooperation Joint Laboratory, as an Assistant Professor, Shenzhen University. He is currently involved in high-speed optical communication technology, optical wireless technology, visible light communication technology, intelligent information processing, and all-optical information devices.



ZEBIN HUANG received the B.S. degree in physics and optoelectronics engineering from Shenzhen University, China, in 2019, where he is currently pursuing the master's degree with the Physics and Optoelectronics Engineering College. His main research interests include intelligent information processing and optical communication based on structured beams.



XIAOMIN ZHANG received the degree from the Department of Optics, Shandong University, in January 1982. After graduation, he is involved in long-term research work on high power solid-state laser technology and engineering. He is a member of the China Optical Association and the Deputy Director of the China Academy of Engineering Physics.



XINXING ZHOU received the B.S. degree in electronic information science and technology from Hunan Normal University, China, in 2010, and the Ph.D. degree in circuits and systems from Hunan University, China, in 2015. He is currently an Associate Professor with Hunan Normal University. His research interests include spin-orbit coupling of light, weak measurements, and optics/photonics. He is an editorial board member of scientific reports.



DIANYUAN FAN received the degree from the Physics Department, Peking University, in 1962. He is a Laser Technology and Engineering Expert and Academician of the Chinese Academy of Engineering, a Researcher of the Shanghai Institute of Optics and Fine Mechanics, Chinese Academy of Sciences, and the Director of the 2D Materials Optoelectronic Technology International Cooperation Joint Laboratory, Shenzhen University. In 1966, he studied at the Institute of Electronics, Chinese Academy of Sciences, and the Shanghai Institute of Optics and Mechanics. After the graduation, he was with the Shanghai Institute of Optics and Fine Mechanics, Chinese Academy of Sciences. In 1995, he was elected as an Academician for the Chinese Academy of Engineering.



YING LI received the Ph.D. degree from Fudan University, China, in 2010. She was a Postdoctoral Fellow of the School of Information Science and Technology, Tsinghua University, from June 2010 to June 2012. She is currently a Professor with the College of Physics and Optoelectronic Engineering, Shenzhen University. She is currently involved in research work on optical communication, microwave photonics, and structured-light field regulation.

...